Title: Aromaticity Effect on Supramolecular Aggregation. Aromatic vs. Cyclic Monohydroxy Alcohols

Author: Natalia Soszka, Barbara Hachuła, Magdalena Tarnacka, Joanna Grelska, Karolina Jurkiewicz, Monika Geppert-Rybczyńska [i in.]

Citation style: Soszka Natalia, Hachuła Barbara, Tarnacka Magdalena, Grelska Joanna, Jurkiewicz Karolina, Geppert-Rybczyńska Monika [i in.]. (2022). Aromaticity Effect on Supramolecular Aggregation. Aromatic vs. Cyclic Monohydroxy Alcohols. "Spectrochimica Acta Part A: Molecular and Biomolecular Spectroscopy" (2022), nr 0, s. 1-19, art. no. 121235. DOI: 10.1016/j.saa.2022.121235

Journal Pre-proofs

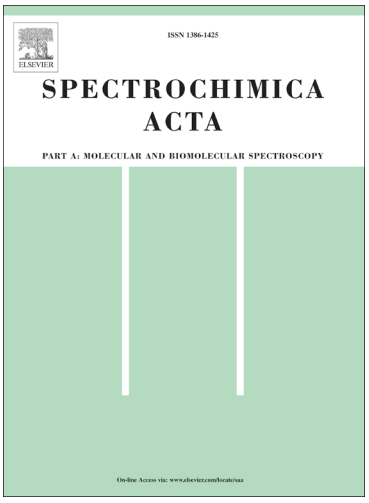

Aromaticity Effect on Supramolecular Aggregation. Aromatic vs. Cyclic Monohydroxy Alcohols

N. Soszka, B. Hachuła, M. Tarnacka, J. Grelska, K. Jurkiewicz, M. Geppert-Rybczyńska, R. Wrzalik, K. Grzybowska, S. Pawlus, M. Paluch, K. Kamiński

PII: S1386-1425(22)00384-5
DOI: https://doi.org/10.1016/j.saa.2022.121235
Reference: SAA 121235

To appear in: *Spectrochimica Acta Part A: Molecular and Biomolecular Spectroscopy*

Received Date: 14 January 2022
Revised Date: 30 March 2022
Accepted Date: 2 April 2022

Please cite this article as: N. Soszka, B. Hachuła, M. Tarnacka, J. Grelska, K. Jurkiewicz, M. Geppert-Rybczyńska, R. Wrzalik, K. Grzybowska, S. Pawlus, M. Paluch, K. Kamiński, Aromaticity Effect on Supramolecular Aggregation. Aromatic vs. Cyclic Monohydroxy Alcohols, *Spectrochimica Acta Part A: Molecular and Biomolecular Spectroscopy* (2022), doi: https://doi.org/10.1016/j.saa.2022.121235

Aromaticity Effect on Supramolecular Aggregation. Aromatic vs. Cyclic Monohydroxy Alcohols

N. Soszka[1,2], B. Hachuła[1*], M. Tarnacka[2], J. Grelska[2], K. Jurkiewicz[2], M. Geppert-Rybczyńska[1], R. Wrzalik[2], K. Grzybowska[2], S. Pawlus[2], M. Paluch[2], K. Kamiński[2]

[1] *Institute of Chemistry, Faculty of Science and Technology, University of Silesia in Katowice, Szkolna 9, 40-006 Katowice, Poland*

[2] *Institute of Physics, Faculty of Science and Technology, University of Silesia in Katowice, 75 Pułku Piechoty 1, 41-500 Chorzów, Poland*

*Corresponding author: (B.H.) barbara.hachula@us.edu.pl

Abstract

In this paper, the steric hindrance effect related to the presence of either an aromatic or cyclic ring on the self-association process in the series of monohydroxy alcohols (MAs), from cyclohexanemethanol to 4-cyclohexyl-1-butanol and from benzyl alcohol to 4-phenyl-1-butanol, was studied using X-Ray Diffraction (XRD), Differential Scanning Calorimetry (DSC), Fourier Transform Infrared (FTIR) spectroscopy, Broadband Dielectric Spectroscopy (BDS) and the Pendant Drop (PD) methods. Based on FTIR results, it was shown that phenyl alcohol (PhA) and cyclohexyl alcohol (CA) derivatives reveal substantial differences in the association degree, the activation energy of dissociation, and the homogeneous distribution of supramolecular nanoassociates suggesting that the phenyl ring exerts a stronger steric impact on the self-assembling of molecules than cyclohexyl one. Additionally, XRD data revealed that phenyl moiety introduces more heterogeneity in the organization of molecules compared to the cyclic one. The changes in the self-association process of alcohols were also reflected in differences in the molecular dynamics of the H-bonded aggregates, as well as in the Kirkwood factor, defining the long-range correlation between dipoles, which were slightly higher for CAs with respect to those determined for PhAs. Unexpectedly it was also found that the surface layers of PhAs were more organized than those formed by CAs. Thus, these findings provided insight into the impact of aromaticity on the self–assembly process, H-bonding pattern, supramolecular structure, and intermolecular dynamics of the studied alcohols.

Keywords: self-association, steric hindrance, phenyl alcohols, cyclohexyl alcohols, aromaticity

Introduction

Aromaticity is one of the most important concept in chemistry, which allows the structural understanding of molecular stability and unusual reactivity of certain carbon-based molecules. This unique property is strongly connected with the presence of the delocalized π electrons in the system. Importantly, interactions involving aromatic rings, such as aromatic $\pi - \pi$ stacking, stabilize the supramolecular architecture, ensure the stability of molecules/biomolecules, participate in biorecognition processes, and are a topic of considerable interest in crystal/material engineering [1,2,3,4,5,6,7,8,9,10,11,12]. These non-covalent forces play an especially important role in self-assembly at the supramolecular level as the aromatic rings can interact in different ways (stacked arrangement, edge- or point-to-face, T-shaped conformation), generating various supramolecular architectures. Such nanostructures can also be affected by halogen substituents which form halogen bonding synthons competing with these molecular contacts.

Aromatic rings, due to their rigidity and planar geometry, can distort the specific attractive interactions, including hydrogen bonds (HBs), and affect the self-assembling of amphiphilic compounds, such as alcohols. In the case of aryl alcohols, the bulky aromatic moiety can be a source of competitive $\pi\cdots\pi$, C−H$\cdots\pi$ and/or O−H$\cdots\pi$ contacts. Many experimental and theoretical investigations focused on the competition between these different interactions that can occur in complexes of substituted aromatic alcohols (phenol and ethynylbenzene [13], $(\text{phenol})_2$ [14] and $(p\text{-cresol})_2$ [15] homodimers; anisole$\cdots$phenol [16], 7-azaindole$\cdots$phenol [17] or *p*-aminophenol$\cdots$*p*-cresol heterodimers [18]), especially to characterized the stabilization driving forces of π-stacked and HB dimers [19,20,21]. On the other hand, the papers devoted to the subject of intra- and/or intermolecular interactions in neat aryl alcohols mainly focused on the study of steric hindrance effect and π electrons on self-assembling phenomena in the liquid phase [22,23,24,25,26,27,28,29,30,31,32]. Firstly, Johari et al. [23] showed that the steric hindrance from the phenyl group in 1-phenyl-1-propanol reduces the extent of intermolecular H-bonding as the Debye-type relaxation process vanishes in this system. Then, the other authors reported that the aromatic ring only affects the supramolecular architecture of associating compounds, i.e., the equilibrium of the ring and chain-like H-bonded structures depends on the mutual distance of the phenyl ring and the

hydroxyl group [26]. Recent work from Nowok and al. [31] also demonstrated that the phenyl ring exerts a much stronger effect on the self-organization of alcohol molecules via the O−H···O scheme than any other type of steric hindrance, leading to a significant decline in the size and concentration of the H-bonded clusters.

In view of the above, it is worth adding that our previous experimental studies of intermolecular interactions in phenyl alcohols also shed new light on the supramolecular self-assembly, structural order, and HB patterns in aromatic systems [33,34]. We reported that HBs could be effectively formed in the series of phenyl alcohols differing in the alkyl chain length, irrespectively of the steric effect of the benzene ring [34]. What is more, their association was primarily governed by the chemical nature of apolar chains. In the case of phenyl derivatives of butyl alcohols, the major factor deciding about the association and nanoordering in self-assemblies was the location of the OH functional group in relation to the carbon skeleton, while the steric hindrance or length of the alkyl side chain does not have a significant influence on the H-bond formation [33]. Thus, our studies signified the modulation of H-bonded alcohol properties and the nanoscale aggregation through aromaticity and persuaded us to extend the study further to other H-bonded compounds having different structural and electronic properties, i.e., cyclic alcohols. This class of alcohols is expected to form H-bonds more easily than their aromatic derivatives due to the high flexibility of the cyclic ring allowing the molecule to acquire open configurations where the hydroxyl group is more exposed and hence more available for H-bonding [22]. In contrast, for phenols, the rigidity of the aromatic ring imposes a unique conformation characterized by the coplanarity of the hydroxyl group and the aromatic ring [22].

Inspired by these results, in this study, we evaluated the influence of the various degree of steric hindrance of the hydroxyl group, aromatic versus non-aromatic, on the self-association ability of alcohols. Moreover, we also analyzed the impact of the length of the alkyl chain on the self-assembling process of non-aromatic cyclic alcohol homologous. To the best of our knowledge, this is the first systematic study on the supramolecular self-assembly of cyclic alcohols in the literature. As all of the lower-order cyclic alcohols form a plastic crystal, until now, they have been mainly investigated for studying glass transition phenomena [35,36,37,38,39]. To deeper examine the steric effects on the H-bond formation in alcohols, we have studied the structural, thermal, and spectroscopic properties of four phenyl alcohols (PhAs; from benzyl alcohol to 4-phenyl-1-butanol) and their cyclohexyl analogs (CAs; from cyclohexanemethanol to 4-cyclohexyl-1-butanol; **Scheme 1**) using Broadband

Dielectric Spectroscopy (BDS), Infrared (IR) Spectroscopy, Differential Scanning Calorimetry (DSC), and X-Ray Diffraction (XRD) techniques. Moreover, the properties of the surface layer were investigated using the pendant drop (PD) method.

Materials and Methods

Cyclic alcohols (cyclohexanemethanol (CM), 2-cyclohexyl-1- ethanol (2C1E), 3-cyclohexyl-1- propanol (3C1P), 4-cyclohexyl-1-butanol (4C1B)) and their phenyl counterparts (benzyl alcohol (BA), 2-phenyl-1-ethanol (2Ph1E), 3-phenyl-1-propanol (3Ph1P), 4-phenyl-1-butanol (4Ph1B)) under investigation (purity > 98%) were purchased from Sigma-Aldrich. Before use, all alcohols were dried under a stream of liquid nitrogen. The chemical structures of the studied alcohols are presented in **Scheme 1**.

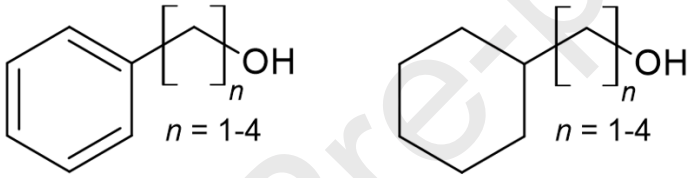

Scheme 1. The chemical structures of (left) aromatic (phenyl) and (right) cyclic (cyclohexyl) alcohols under investigation.

Broadband Dielectric Spectroscopy (BDS)

BDS measurements were carried out on heating after a fast quenching of the liquid state in a wide range of temperatures (159 – 303 K) and frequencies (10^{-1} – 10^{6} Hz) using Novocontrol spectrometer, equipped with Alpha Impedance Analyzer with an active sample cell and Quatro Cryosystem. The samples were placed between two stainless-steel electrodes (diameter: 15 mm, gap: 0.1 mm) and mounted inside a cryostat. During the measurement, each sample was maintained under dry nitrogen gas flow. The temperature was controlled by Quatro Cryosystem using a nitrogen gas cryostat, with stability better than 0.1 K.

The collected dielectric spectra were analyzed by the superposition of Havriliak-Negami (HN) function with the dc-conductivity term [40] to determine the relaxation times of the Debye process, τ_D:

$$\varepsilon * (\omega) = \frac{\sigma_{dc}}{\varepsilon_0 \overline{\omega}} + \frac{\Delta\varepsilon}{\left[1 + (i\omega\tau_{HN})^{\alpha_{HN}}\right]^{\beta_{HN}}}, \quad (1)$$

where α_{HN} and β_{HN} are the shape parameters representing the symmetric and asymmetric broadening of given relaxation peaks, $\Delta\varepsilon$ is the dielectric relaxation strength, τ_{HN} is the HN relaxation time, ε_0 is the vacuum permittivity, and ω is an angular frequency ($\omega = 2\pi f$). Note that all τ_D were estimated from τ_{HN} accordingly to the equation given in Ref. [41].

Additionally, the stretching parameter β_{KWW}, which is usually used to describe the Full Width at Half Maximum (FWHM) of the α-loss peaks, has been determined from the α_{HN} and β_{HN} parameters from the following equation [42]:

$$\alpha_{HN}\beta_{HN} = \beta_{KWW}^{1.23} \quad (2)$$

It was found that β_{KWW} ~ 0.91-96 (see **Table 1**). Note that the fitting procedure was performed using only one HN function, as the application of additional mode was unreliable, and the fitting parameters of the second HN function changed non-monotonically with the temperature. Alternatively, the value of the stretched exponent, β_{KWW}, was determined from the fitting of chosen spectra to the one-sided Fourier transform of the Kohlrausch-Williams-Watts (KWW) function [43,44].

To determine the glass transition temperatures of all studied CAs, the estimated τ_D were fitted by the Vogel-Fulcher-Tammann (VFT) equation [45,46,47]:

$$\tau_D = \tau_\infty exp\left(\frac{D_T T_0}{T - T_0}\right), \quad (3)$$

where τ_∞, D_T and T_0 are the fitting parameters. Note that T_g is defined as a temperature at which τ_D = 100 s.

Refractive index measurements

The refractive index, n, measurements of the studied liquids were carried out using the Mettler Toledo refractometer RM40 in the temperature range 293−343 K. The temperature stability controlled with the aid of a built-in Peltier thermostat was better than 0.1 K. The light source is a light-emitting diode, the beam of which passes through a polarization filter, an interference filter (589 nm), and various lenses before it reaches the sample via the sapphire

prism characterized by high thermal conductivity. The measurements of n were performed with a resolution of 0.0001. The determined values are presented in **Figure S1** (please see the **Supplementary Material** (**SM**) file). Note that the values of n parameter used to calculate the Kirkwood correlation factor (g_K) at $T = T_g + 10$ K were estimated according to the linear fit of the measured data.

Differential Scanning Calorimetry (DSC)

Calorimetric measurements were carried out by Mettler-Toledo DSC apparatus equipped with a liquid nitrogen cooling accessory and an HSS8 ceramic sensor (heat flux sensor with 120 thermocouples). Temperature and enthalpy calibrations were performed by using indium and zinc standards. The sample was prepared in an open aluminum crucible (40 μL) outside the DSC apparatus. Samples were scanned at various temperatures at a constant heating rate of 10 K·min^{-1}.

X-ray Diffraction (XRD) Scattering

The wide-angle XRD patterns were collected using a Rigaku Denki D/MAX Rapid II-R diffractometer equipped with a rotating Ag anode, a graphite (002) monochromator, and an image plate detector in the Debye–Scherrer geometry. The wavelength of the incident beam, λ , was 0.5608 Å. The beamwidth at the sample was 0.3 mm. Each sample was measured at room temperature of around 293 K and around the glass transition temperature, in transmission geometry, in borosilicate glass capillaries having 1.5 mm in diameter and 0.01 mm of wall thickness. The temperature was controlled using Oxford Cryostream 800 cooler. The total X-ray scattering data were collected in the range of the scattering vector $Q = \frac{4\pi sin\theta}{\lambda}$ (where 2θ is the scattering angle) of 0.25 – 20 Å^{-1} and corrected for background. Comparison of the X-ray scattering data for CAs and PhAs in the full-measured Q range of 0.25 – 20 Å^{-1} is shown in the **SM** file in **Figure S2**.

Fourier Transform Infrared (FTIR) spectroscopy

FTIR spectra were recorded using a Thermo Scientific Nicolet iS50 spectrometer with a resolution of 2 cm^{-1} (16 scans) in the spectral range of 400–4000 cm^{-1}. The spectrometer

was equipped with a Linkam THMS 600 heating/cooling stage (Linkam Scientific Instruments Ltd., Surrey, UK) which allowed us to execute the temperature measurements in the range 373–93 K for CM, 368–133 K for 2C1E, 3C1P, and 4C1B applying the rate of 5 K min^{-1}. The spectra were collected every 5 K in transmission mode. To obtain samples of uniform thickness and absorbance value, a liquid cell with two CaF_2 windows separated by the 6 μm thick Mylar spacer was used. Throughout the experiment, liquid nitrogen was passed through the spectrometer to avoid atmospheric H_2O and CO_2 bands in the spectrum. Moreover, FTIR spectra of alcohol solutions in carbon tetrachloride (CCl_4) were also collected in the frequency range 400-4000 cm^{-1} using a transmission solution cell with KBr windows and a path length of 1.03 mm. The solutions were prepared by serial dilution of a 0.1M solution down to 0.0001M. A total of 16 scans with a spectral resolution of 2 cm^{-1} were averaged for each sample. The MagicPlotPro software (version 2.9.3, MagicPlot Systems LLC, Saint Petersburg, Russia) was used to perform the deconvolution process of the OH stretching bands, enabling the determination of activation enthalpy for cyclic alcohol dissociation. The step-by-step process of the OH stretching band decomposition was described in our previous work [33] and in the **SM** file.

Surface tension measurements

The density of the investigated CAs was measured using Anton Paar DMA 5000M densimeter. Condition for these measurements has been previously described in the previous paper [34] (the standard uncertainties are $u(p) = 1{\cdot}10^{-2}$ MPa and $u(T) = 0.01$ K, and the combined expanded uncertainty of the density is $u(\rho) = 5{\cdot}10^{-4}$ g cm^{-3} (at 0.95 confidence level ($k \approx 2$)). The temperature range for density measurements was $T = (283.15 – 323.15)$ K, with a step of 10 K and at 298.15 K. Based on density temperature dependence, it was possible to calculate density at lower temperatures necessary for surface tension measurements and the calculation of Kirkwood factor, g_k. The density of CAs and PhAs [34] was presented in **Figure S3**. This comparison shows that the density of CAs is significantly lower than that of PhAs.

The surface tension was measured using the pendant drop method with the Drop Shape Analyzer DSA 100S - the Krüss Tensiometer (equipped with Advance Software). The instrumental description as well as all procedures have been described previously [34,48,49]. The general T range was (298.2 – 267.6) K with variable steps at a minimum of 4 temperatures. The general uncertainty of the method was 0.2 mN m^{-1}, but in our case, the

standard deviation of the mean value was for three first homologues below 0.6 mN m^{-1} and only for 4-cyclohexyl-1-butanol at 273.2 K was around 1 mN m^{-1}. Based on the instrument standard uncertainty and the standard uncertainties in pressure, $u(p) = 1{\cdot}10^{-2}$ MPa, temperature and $u(T) =$ 0.1 K and density, $u(\rho) = 5{\cdot}10^{-4}$ g cm^{-3}, the average combined expanded uncertainty $u(\gamma)$ (at 0.95 level of confidence, $k = 2$) was not worse than 1 mN m^{-1}. The surface tension of CAs is presented in **Figure 5(a)**, whereas a comparison of γ with those of PhAs [34] and aliphatic alcohols (AAs) [50,51] at T = 298.2 K, is drawn in **Figure 5(b)**. Moreover, in **Figure 5(c)** and **5(d)**, the surface entropy ($S^a = -\left(\frac{\partial\gamma}{\delta T}\right)_p$, 10^{-3} mN m^{-1} K^{-1}) and the molar surface entropy ($S_v = -8.45 \cdot V_m^{2/3}{\cdot}\left(-\frac{\partial\gamma}{\delta T}\right)_p$, J K^{-1} mol^{-1}, where V_m is the molar volume) are presented, respectively. These quantities are calculated based on the temperature dependence of surface tension. **Figure 5** includes also S^a and S_v of PhAs[34], AAs and alkanes [50,51,52].

Density functional theory (DFT) computations

Density functional theory (DFT) calculations using the B3LYP functional, combined with the 6-311+G(2d,p) basis set, were performed within the Gaussian09 software package [53]. The geometries of benzene and benzyl alcohol dimers were optimized with the Opt = Tight option. The counterpoise method was used to correct the interaction energies (ΔE_{BSSE}) for the basis set superposition error (BSSE) [54].

Results and discussion

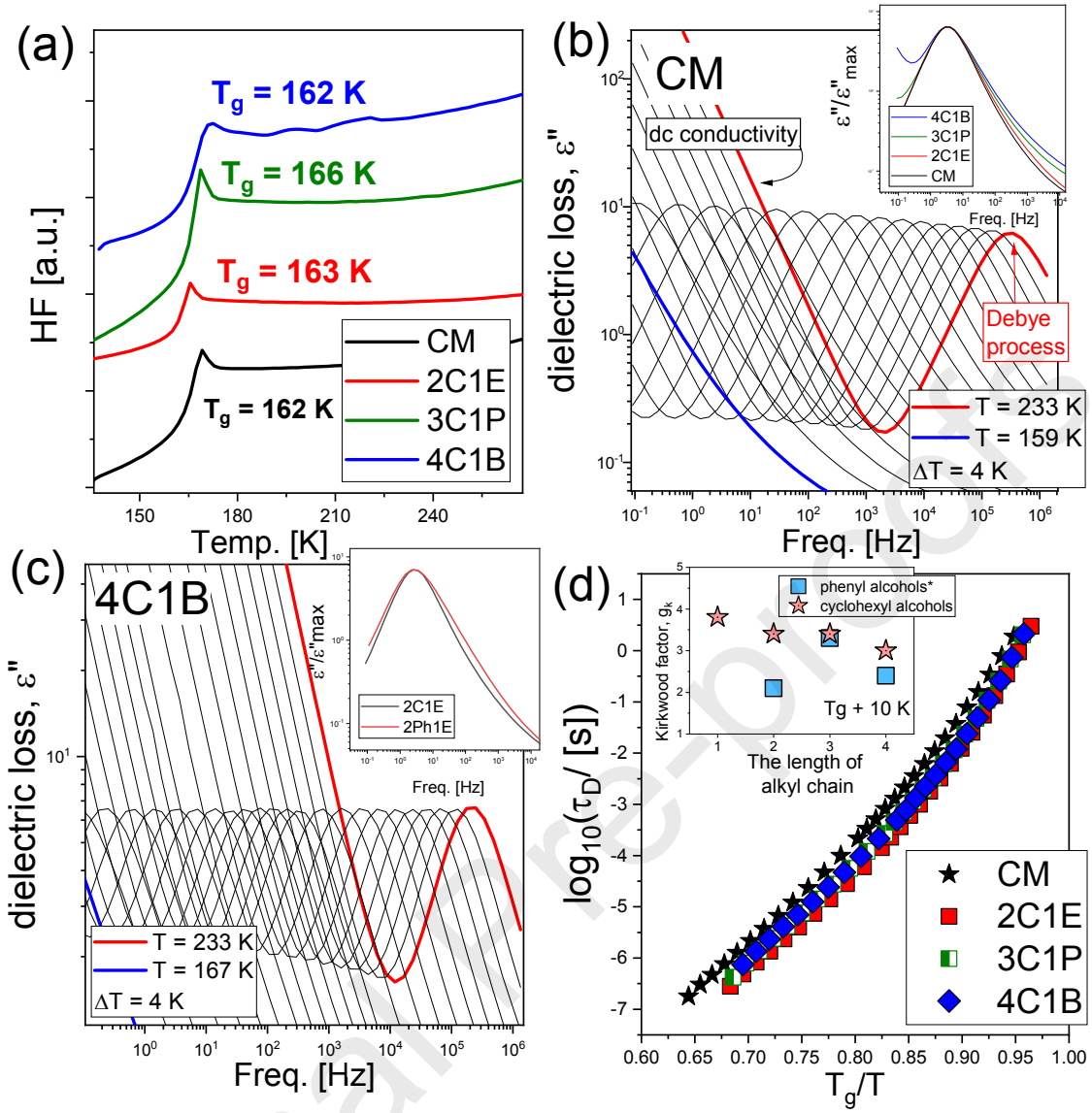

Figure 1. (a) DSC thermograms collected for indicated CAs. (b, c) Dielectric loss spectra of (b) CM and (c) 4C1B were measured above their glass transition temperatures. The insets of panels (b) and (c) show the comparison of dielectric loss measured spectra at constant τ_D near T_g of all examined CAs and the comparison between 2Ph1E and 2C1E, respectively. (d) Temperature dependences of the relaxation times of Debye-like process, τ_D, determined for the examined CAs, plotted as a function of T_g/T. As the inset in panel (d), values of the Kirkwood factor, g_K, determined at $T_g + 10\ K$ plotted as a function of the length of the alkyl chain of examined CAs. *Data for PhAs were taken from Ref. [34].

Table 1. Molar mass (M) of examined CAs, glass transition temperature (T_g, determined from calorimetric and dielectric measurements), as well as values of the stretched exponent (β_{KWW}), the Kirkwood factor (g_k, calculated at $T = T_g + 10$ K), dipole moment (μ, obtained from DFT calculations), and the refractive index (n, measured at 303 K).

Sample	M [g mol^{-1}]	$T_{g,DSC}$ [K]	T_g [K] for τ_D = 100 s	β_{KWW}	g_k at $T_g + 10K$	μ [D]	n at 303 K
CM	108.14	162±2	157±2	0.96±0.1	3.8	1.523	1.460
2C1E	122.16	163±2	159±2	0.95±0.1	3.4	1.613	1.461
3C1P	136.19	166±2	160±2	0.94±0.1	3.4	1.537	1.462
4C1B	150.22	162±2	162±2	0.91±0.1	2.9	1.652	1.463

At first, we start our investigation with the calorimetric measurements in order to reveal all possible phase transitions in the studied materials. The recorded DSC curves are shown in **Figure 1(a)**. As illustrated, all samples exhibit one pronounced jump in their heat capacity related to the glass transitions located at 162-166 K, defined as the glass transition temperature, T_g. Interestingly, the estimated T_gs are basically independent of the alkyl chain length in the examined CAs, revealing no molecular mass, M, dependence, see **Figure 1(a) and Table 1**. In this context, one can recall recent studies on the series of non-aromatic MAs, which revealed that their T_g increases with M [31,55]. However, it should be highlighted that those reports considered various MAs isomers of more complex chemical structure, whereas herein, we focused only on cyclohexyl-substituted MAs characterized by linear structure and a different number of -CH_2- groups (see **Scheme 1**), in contrast to the previous investigations [31]. Nevertheless, one can mention that the values of T_gs determined for examined CAs are significantly lower when compared to the ones reported previously for their aromatic counterparts, phenyl-substituted MAs (PhAs). Note that T_gs of PhAs change in range of 181-184 K [26,27,34] (see **Figure 6(a)**). In this context, one can assume that the examined CAs are characterized by T_gs comparable rather to the aliphatic alcohols than PhAs. This implies that the aromaticity of the side group has a significant impact on the glass transition of MAs.

Taking all of those observations into account, we wonder if the varying length of the alkyl chain of CAs would affect the molecular dynamics of these compounds and how it would be different compared to their aromatic counterparts. Thus, we performed additional dielectric measurements. Representative dielectric loss spectra measured for two selected

CAs, cyclohexanemethanol (CM) and 4-cyclohexyl-1-butanol (4C1B), are shown in **Figure 1(b,c)**. As illustrated, one can distinguish two dielectric processes, dc conductivity (at lower frequencies) and Debye like, D, process (at high frequencies), see **Figure 1(b,c)**. Both of them shift toward lower frequencies with decreasing temperature. Note that the value of the stretched exponent, β_{KWW}, reaches ~ 0.91-0.96 (all values are listed in **Table 1;** β_{KWW} was determined from the shape parameters of the Havriliak-Negami (HN) function with an additional conductivity term [40] used to fit recorded loss spectra – details are shown in the **Experimental section**). These values clearly confirmed that the dominant process observed in **Figure 1(b,c)** for all examined CAs has the Debye-like character ($\beta_{KWW} \approx 1$). At this point one can also mention that the determined values of β_{KWW} parameter for CAs are comparable to those previously reported for their aromatic counterparts, where β_{KWW} ~ 0.90-0.95 [26,27,34]. One can recall that the presence of the exponential decay of the electric polarization (*D*-relaxation), characterized by a single time constant, is considered as a characteristic feature for some associating liquids, including in MAs having hydroxyl unit(s) attached to the terminal carbon [56]. Note that often for those materials, the Debye mode dominates the recorded dielectric response [57,58], resulting in that the structural α-relaxation is reflected only as an excess wing on the *D*-peak's high-frequency flank. It should be mentioned that although the molecular mechanism of the Debye relaxation remains a puzzle [59,60,61,62,63], recently, this unique dielectric mode has been generally discussed in terms of the variation of the formed hydrogen bonds, including migration of defects through the H-bonded network [27], dissociation process [64] or the transition from the ring to the linear architecture of supramolecular structures as deduced from dielectric measurements carried out in the nonlinear regime [65]. Therefore, by analyzing the shape, the dielectric strength, $\Delta\varepsilon$, and the relaxation times, τ, of *D*-process, one can gain some indirect insights into the population and behavior of H-bonds and morphology of associates.

In the inset of **Figure 1(b)**, we plotted the dielectric loss spectra measured for all studied CAs and characterized by the same relaxation times of the Debye like process, τ_D (representative loss spectra were arbitrarily shifted vertically to superpose at maximum). Interestingly, we observed a broadening of the distribution of relaxation times with the length of the alkyl chain of studied materials. It might imply some variation in the H-bonded structures formed by examined series of CAs due to an increasing alkyl chain (an increasing molecular mass). Surprisingly, a comparison of loss spectra of 2C1E (non-aromatic MA) and 2Ph1E (aromatic MA) superposed at constant τ_D also shows that there are some differences

between both classes of MA. As shown, the distribution of relaxation times of PhAs is slightly broader when compared to their non-aromatic counterparts; see the insert in **Figure 1(c)**. This broadening might arise due to a different timescale between the structural (α) and *D* modes [26,27] (or alternatively due to the varying dielectric strength of both modes), as a result of the variation within the population of HB between both classes of materials (especially in terms of its heterogeneous nature). The differences in the behavior of the HB population arose due to variation in the chemical structure of examined MA will be investigated further by means of IR spectroscopy in the latter part of the manuscript.

Furthermore, we determined the values of glass transition temperature from the dielectric data. In **Figure 1(d),** we have shown the relaxation times of the Debye like mode, τ_D, plotted as a function of T_g/T. Note that all τ_D were determined from fits of recorded loss spectra to the HN function with an additional conductivity term [40] (see **Experimental section)**. The obtained $\tau_D(T)$-depencences were further fitted to the Vogel-Fulcher-Tammann (VFT) equation in order to determine the values of $T_g s$ of examined compounds (see **Experimental section**). All estimated values of T_g (defined as T at which τ_D= 100s) are added in **Table 1**. As it can be seen, $T_g s$ determined from $\tau_D(T)$-depencences are a few degrees lower (0-6 K) than those obtained from calorimetric studies. Note that this might be due to the different heating rates applied in both techniques.

Taking advantage of performed dielectric measurements, we calculated the Kirkwood correlation factor (g_K), which provides useful information about the variation in the local molecular arrangement in the studied CAs. The g_K parameter was estimated as follow [66]:

$$g_k = \frac{9k_B\varepsilon_0 MT(\varepsilon_s - \varepsilon_\infty)(2\varepsilon_s + \varepsilon_\infty)}{\rho N_A \mu^2 \varepsilon_s(\varepsilon_\infty + 2)^2}, \qquad (4)$$

where: k_B is the Boltzmann constant (~1.38 × 10^{-23} m^2 kg s^{-2} K^{-1}), N_A is Avogadro's number (~6.022 × 10^{23}), ρ is density, μ is molecular dipole moment determined from Density Functional Theory (DFT) computations, whereas ε_s and ε_∞ are static permittivity and permittivity at infinite frequencies, respectively. Note that the ε_s parameter was taken from BDS data, while the ε_∞ one was estimated from refractive index (n) measurements (where $\varepsilon_\infty \sim n^2$, the temperature dependence of n is shown in **Figure S1**). The temperature dependences of g_K parameter are presented in **Figure S4,** whereas those calculated at $T = T_g + 10$ K are shown in the inset in **Figure 1(d)** and **Figure 5(b)**. As illustrated, g_K ~ 3-4 for all examined CAs in the whole range of experimental data. Moreover, g_K increases upon cooling, as was

previously reported for various aromatic alcohols [26,27,34] as well as aliphatic MA, i.e., isomers of butanol [67]. One can recall that taking into account the Dannhauser approach, the value of $g_K > 1$ indicates cross-correlation between chain-like aggregates in self-assembling systems [68,69,70]. However, it should be mentioned that the value of g_K decreases with the elongation of the length of the alkyl chain in the structure of CAs. Note that the highest and the lowest value of g_K were reached for CM and 4C1B, respectively (see the inset in **Figure 1(d)**). This might indicate that an increasing alkyl chain (and therefore molecular weight) of CAs disturbs the formation of chain-like self-assembles. Nevertheless, it should be highlighted that the linear decrease of g_K as a function of an increasing number of -CH_2- groups observed for CAs is opposite to the one observed for PhAs. As reported, g_K determined for phenyl-substituted MA revealed a clearly non-monotonic variation with the increasing length of the alkyl group, where the maximum (the highest value of g_K) was noticed for 3Ph1P [34]. Therefore, one can assume that there are some significant differences in the strength and population of self-assemblies formed by either aromatic or non-aromatic alcohols. To follow, in detail, differences in the behavior of HBs arose due to variation in the chemical structure of examined MA, further FTIR studies were performed.

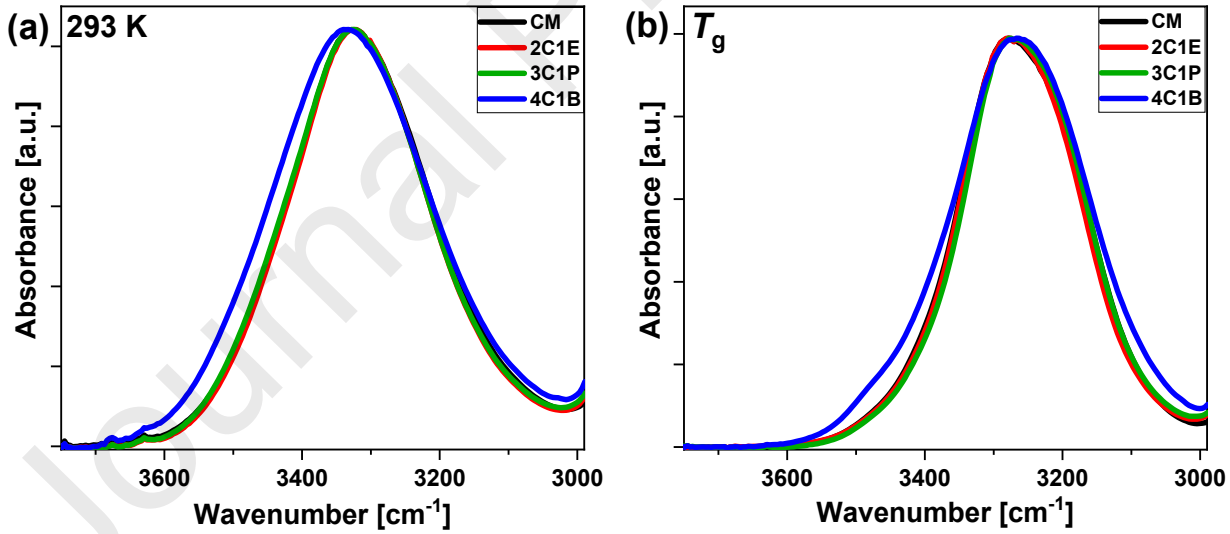

Figure 2. FTIR spectra of CAs in the frequency range 3750-2990 cm^{-1} measured at (a) 293 K and (b) T_g. The spectra were normalized to the maximum intensity of OH stretching vibration.

To shed light on the dynamics of hydrogen bonds (HBs) in alcohols and to better understand/recognize the influence of the aromatic ring on the assembling phenomenon, special attention was paid to FTIR spectra of CAs and their phenyl analogs in the OH stretching (υ_{OH}) vibrational region. It should be noted that the impact of the length of the alkyl

side chain on the behavior of benzyl alcohol homologues was studied in detail in our previous paper [34]. The representative FTIR spectra for CAs at selected temperatures (the room temperature, RT = 293 K, and T_g) in the region of 3750-2990 cm^{-1} are presented in **Figure 2**. Characteristic peaks, appearing at ~3330 cm^{-1} and 3629 cm^{-1} at RT, are assigned to the stretching vibration of the hydrogen-bonded (ν_{OH}^{HB}) and non-hydrogen-bonded 'free' (ν_{OH}^{free}) hydroxyl groups, respectively. The band assignment of the last one is additionally confirmed by the measurements of solutions of CAs in various non-polar solvents (cyclohexane, carbon tetrachloride (CCl_4), benzene) (**Figure S5** in the **SM** file). Based on **Figure S5**, one can also see that the type of solvent influences the self-assembly process of alcohols under investigation. In addition, the association of CAs in CCl_4 depends on the alkyl chain length, i.e., the ν_{OH}^{HB} band profile changes with the elongation of the chain length (the different intensity ratio of peaks at ca. 3490 cm^{-1} and 3350 cm^{-1}). On the other hand, for diluted solutions of CAs in cyclohexane and benzene, the lengthening of the side chain does not vary the spectral properties of ν_{OH}^{HB} band. As presented in **Table S1**, up to the $x = 3$ (where x is the number of CH_2 units in the hydrocarbon side chain), the frequencies of ν_{OH}^{HB} band at 293 K are comparable (these data were obtained from the band deconvolution of FTIR spectra with the use of Gaussian–Lorentzian functions in OMNIC software; **Figure S6** in the **SM** file), implying a similar strength of HBs in these systems. On the other hand, the value of ν_{OH}^{HB} frequency for 4C1B deviates from the others, i.e., HBs between 4C1B molecules are slightly weaker than for shorter CAs. With the decreasing of temperature, the red-shift of ν_{OH}^{HB} bands is observed which indicates the weakening of the OH-bonds due to the formation of stronger HBs. Interestingly, when comparing the frequencies of the ν_{OH}^{HB} signals of CAs in both temperatures, it is seen that the intermolecular interactions in 4C1B are the weakest among all CAs at RT, but the situation changes at T_g when they become the strongest ones. Moreover, on cooling, the ν_{OH}^{free} band disappears confirming nearly complete/total association of CA molecules at T_g. On the other hand, the estimation/calculations of the non-bonded OH moieties' percentages in CAs at RT (**Figure S8(a)**) shows that the population of the H-bonded OH groups decreases, while that of the free OH increases (from 0.54% to 1.05%) with the elongation of the chain length. Such a small fraction of non-associated (monomeric) molecules was also identified in aliphatic alcohols (< 2% in methanol and even less in other alcohols) [71]. Therefore, the degree of self-association of CAs slightly decreases with the increase in the side chain length. A similar spectral effect was detected for aliphatic 1-alcohols in the liquid phase by Kwaśniewicz and Czarnecki [72].

Next, an analysis of the bandwidth of OH stretching vibration measured by the full width at half maximum, $FWHM$, was conducted. Herein it should be stressed that $FWHM$s of the ν_{OH}^{HB} bands were obtained as parameters from the curve fitting using Gaussian–Lorentzian functions in OMNIC software (see **Figure S6**). It can be clearly seen that $FWHM$ values are essentially similar for the first three CAs at RT. However, it considerably changes in the case of 4C1B, i.e., $FWHM$ is greater than for the others (ca. 30 cm^{-1}) at RT. This indicates that the most heterogeneous aggregates in terms of HB strength are formed in 4C1B. Therefore, one can state that the length of the alkyl side chain starts to affect the distribution of H-bonded networks significantly for longer cyclic alcohols, i.e., when the $x = 4$. Such behavior may suggest the competition between the dispersive and HB interactions as the length of alkyl units increases. At T_g, $FWHM$s generally take smaller values suggesting that more ordered and homogeneous supramolecular nanoassociates are formed (**Table S1**).

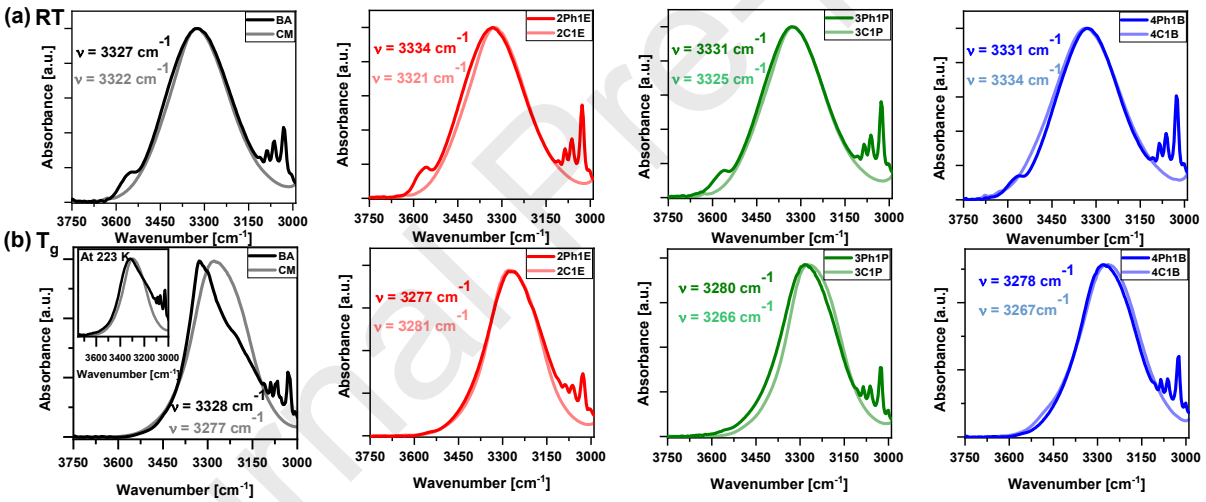

Figure 3. Comparison of CAs and PhAs at (a) 293 K and (b) T_g in the spectral range of 3750-2990 cm^{-1}. The inset shows the ν_{OH}^{HB} bands at 223 K (at temperature just before crystallization of BA). The spectra were normalized with respect to the absorbance maximum of the OH stretching vibration peak.

Further, to discuss/reveal the role of aromaticity in alcohol self-assembly, the spectral properties of CAs and PhAs were compared. FTIR spectra of both CAs and PhAs in the range 3750-3000 cm^{-1} at RT and T_g are presented in **Figure 3**. At first glance, the clear difference in the amount of non-bonded OH moieties is visible for the studied alcohols at 293 K, that is, the intensity of ν_{OH}^{free} is much higher in the spectra of aromatic alcohols compared to the cyclic

ones (**Figure 3(a)**). It indicates that the aromatic ring indeed acts as a steric hindrance and prevents molecules from forming HB aggregates to a greater extent compared to CAs. As can be seen from **Table S1**, the shortest alcohols, CA and BA, are characterized by the strongest interactions at RT (the lowest frequency of the ν_{OH}^{HB} band). For CAs, the HB strength decreases with an elongation of the chain length at RT. Interestingly, the same effect was observed for neat aliphatic 1-alcohols, i.e., the hydrogen bonding weakens with the chain length increase [72]. It is of note that the opposite trend is observed for CAs at T_g. In the case of PhAs, a non-monotonic change in HB strength, as the length of the alkyl chain grows, occurs at both temperatures (the weakest HB interactions for 2Ph1E at RT and 3Ph1P at T_g). This irregular spectral variation for PhAs indicates a strong change in the assembling mechanism going from shorter to longer PhAs resulting from an interplay between dispersive and HB interactions [34]. Similar behavior was detected in the case of protic ionic liquids (PILs), in which the lengthening of the cation alkyl chain leads to well-defined self-assembled nanostructures in which the polar and apolar domains were better segregated [73]. Nanostructure in PILs results from electrostatic and H-bonding attractions between charged groups leading to the formation of polar domains. Cation alkyl groups are repelled from these regions and forced to cluster together into apolar regions.

An analysis of the $FWHMs$ of studied alcohols at both temperatures clearly shows that the shorter PhAs (up to the x = 3) have a broader ν_{OH} bands than CAs, which suggests the existence of additional interactions involving aromatic rings apart from the typical $O-H\cdots O$ contacts. The existence of such competitive type of H-bonds, $O-H\cdots\pi$, was also suggested by DFT calculations ($O-H\cdots O$ (ΔE_{BSSE} = -5.67 kcal·mol^{-1}) vs. $O-H\cdots\pi$ (ΔE_{BSSE} = -2.06 kcal·mol^{-1}); **Figure S7**). Interestingly, there is a reverse relationship for butanols, i.e., $FWHM$ of 4C1B is considerably greater than 4Ph1B. Therefore, it can be concluded that HBs of shorter CAs (x=1-3) are more homogeneous (the interactions are similar in strength) than those of PhAs. This property also changes with the chain length for PhAs, i.e., their ν_{OH}^{HB} bands at RT narrow with the elongation of the alkyl chain. The opposite is true at a lower temperature (T_g).

Further, we performed the calculations of the activation enthalpy (E_a) for the dissociation of CAs using the van't Hoff equation, according to the procedure described in our previous work, and compared them with the values obtained for PhAs [34]. **Figure S8(b)** shows that CAs exhibit a non-monotonic relationship between E_a values and the number of

CH_2 units in the side chain, i.e., the maximum value of E_a occurs for 2C1E (24.58 kJ mol^{-1}). In contrast, a clear increase in the E_a values with a chain extension is observed for PhAs. What is more, the E_a values of CAs are much higher than those of phenyl derivatives (~10 kJ mol^{-1}). It might be related to the higher flexibility of cyclohexyl ring, for which much more comfortable conformations can be adapted, resulting in an increased HB stabilization. It should also be mentioned that the average enthalpies of H-bonding for methanol, ethanol, propan-1-ol, propan-2-ol, butan-1-ol, hexan-1-ol and octan-1-ol in the liquid phase are in the range from - 15.1 to - 17.7 kJ mol^{-1} [71]. Thus, these values are between those obtained for CAs and PhAs. We also determined the average number of molecules in H-bonded aggregates of CAs based on the investigation of alcohols in dilute CCl_4 solution using the method described in the **SM** file. As presented in **Table S2**, CAs form the supramolecular assemblies (n) containing 3 or 4 H-bonded molecules, whereas the $n \sim 3$ for PhAs. Consequently, at RT the trimers and tetramers dominate in CAs.

Based on the performed FTIR studies, we observed that the elimination of aromaticity in the examined monohydroxy alcohols, made by a simple substitution of phenyl ring by non-aromatic cyclohexyl one, leads to some pronounced difference in the strength and the population of formed hydrogen bonds network. To support these observations concerning the differences in the HB distribution in the studied materials as an effect of side group aromaticity, further structural studies were performed.

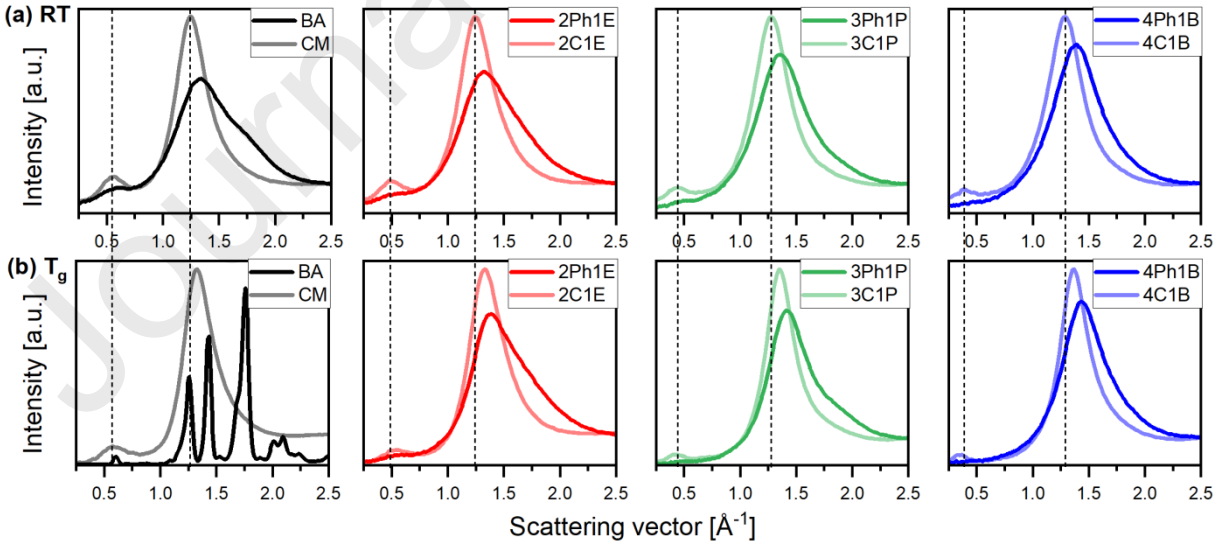

Figure 4. Comparison of XRD data for CAs and PhAs at (a) 293 K and (b) T_g in the low-Q range of 0.25 – 2.5 Å^{-1}. The data for PhAs were normalized to the maximum of the main peak, while the data for each CA were normalized to the high-Q range (5 – 20 Å^{-1}) of the corresponding PHA.

The differences in the supramolecular structure between the studied alcohols are also revealed in the X-ray diffraction (scattering) patterns. **Figure 4(a)** shows the comparison of the scattering data in the low-Q range up to 2.5 Å^{-1} for the four pairs of cyclic alcohols and their phenyl analogues, as a function of alkyl chain length looking from left to right. The diffractograms for CAs in this range are characterized by two features related to the intermolecular structure: the main peak around 1.25 Å^{-1} and the pre-peak around 0.5 Å^{-1}. The origin of the pre-peak in alcohols has been discussed in many papers [74,75,76,77] and explained based on the computer simulations as arising due to structural correlations between OH groups as a consequence of the association of molecules by HBs. One can see that the intensity of the pre-peak decreases, the width increases, while its position shifts towards lower Q values with the elongation of the chain for CAs. It means that the correlation distances move towards greater values and the total intermolecular correlations weaken on this length scale for longer CAs. Since the correlations in the pre-peak region for alcohols are mainly due to OH groups, it indicates a weakening of the association of CAs via HBs with the increase in the chain length.

The X-ray scattering data for PhAs show clear differences compared to their cyclic analogs: (*i*) the main peak is much wider, less-intense, asymmetric and shifted towards higher Q values, (*ii*) the pre-peak is damped. In fact, the pre-peak is clearly visible only for the shortest PhA – BA. With the increase of the chain length, the pre-peak is suppressed. A similar tendency was observed for CAs. For the 4Ph1B, the pre-peak completely disappears. It means that the supramolecular correlations on the medium-range scale are missing, or the partial atomic correlations cancel each other out. The explanation of this phenomenon may be possible based on the computer simulations. Nevertheless, such a difference in the scattering patterns between the cyclic and aromatic alcohols suggests that the aromaticity introduces more heterogeneity into the intermolecular structure. This is also confirmed by the behavior of the main peak related to the short-range intermolecular correlations. It is clearly seen that the main peak is more asymmetric and its *FWHM* is much wider for aromatic alcohols than for cyclic counterparts. The asymmetry of the main peak suggests that it is composed of two overlapping components. That would indicate two preferred arrangements of molecules. It would be possible when the phenyl ring stacking occurs. The presence of two competitive organization of molecules, via the π-related interactions and H-bonding, would introduce two different periodic lengths, i.e. a larger distance between molecules (comparable to the intermolecular distance in CAs) as well as a smaller distance related to the phenyl ring stacking. Therefore, the short-range structure of PhAs can be considered more heterogeneous

than CAs. The differences in the position and full-width at half maximum of the main diffraction peak for CAs and PhAs are presented in Fig. 4 (a,b).

Figure 4(b) shows the XRD patterns for the studied alcohols measured at temperatures around T_g. BA crystallized at this condition. For the other alcohols, the positions of the main peak shift towards higher Q values (smaller distances) with the temperature drop. This is the standard temperature effect. The $FWHM$ values also behave as standard – decrease for lower temperatures, indicating an increase in the degree of structural order and coherence length.

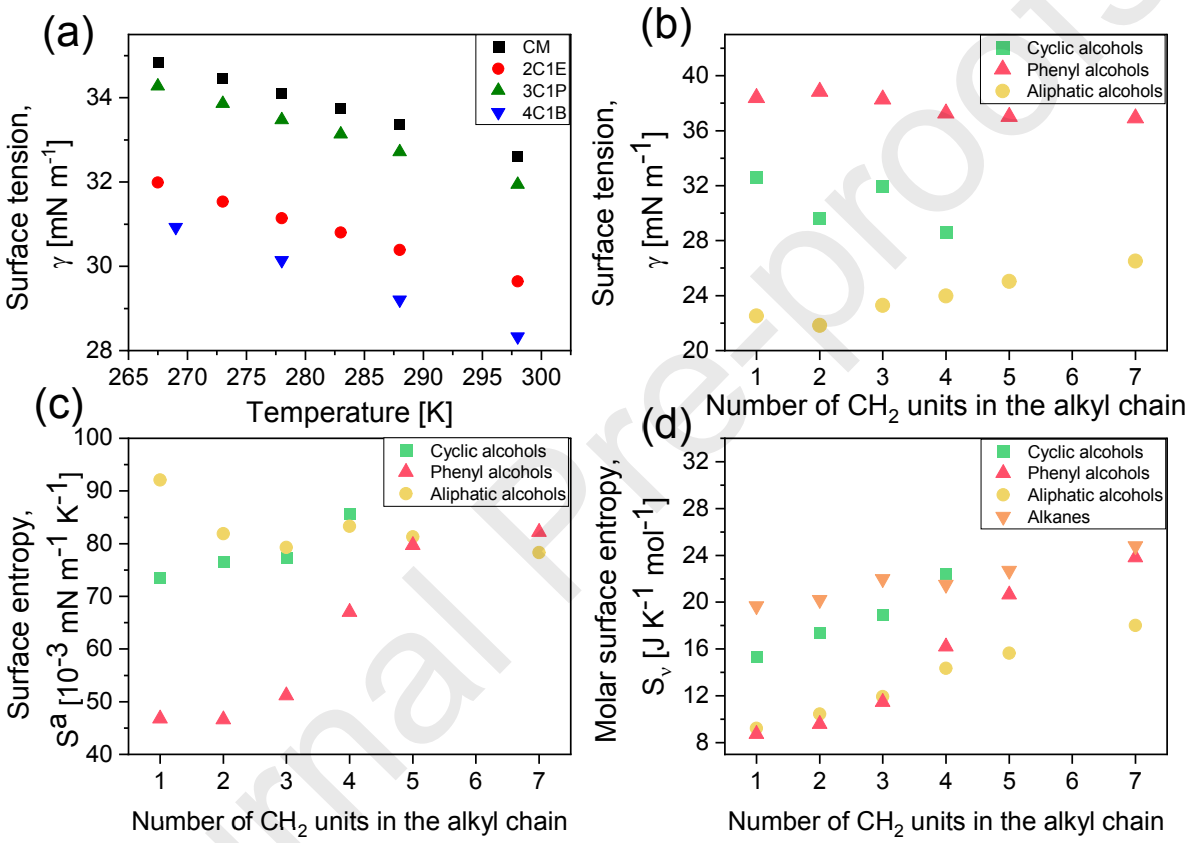

Figure 5. (a) Surface tension of CAs at different temperatures T. (b) Comparison of surface tension of CAs with γ of PhAs[34] and aliphatic alcohols [50,51] at $T = 298.2$ K. (c) Surface entropy ($S^a = -\left(\frac{\partial\gamma}{\delta T}\right)_p$, 10^{-3} mN·m^{-1}·K^{-1}) of CAs compared with S^a of PhAs[34] and aliphatic alcohols [50,51]**Error! Bookmark not defined.**. (d) Molar surface entropy ($S_v = -8.45 \cdot V_m^{2/3} \cdot \left(-\frac{\partial\gamma}{\delta T}\right)_p$, J·K^{-1}·mol^{-1}) of CAs compared with S_v of PhAs[34], aliphatic alcohols and alkanes[52].

To obtain more information about the behavior of alcohols differentiated in terms of the side groups (aromatic or non-aromatic), we also measured their surface tension, γ, and calculated the surface entropy, S^a, as well as molar surface entropy, S_v, which is supposed to

allow us to distinguish these materials according to the intermolecular forces. The estimated values of S^a, S_v, and γ at different temperatures are shown in **Figure 5** and are listed in **Table S3**. It can be noticed that previously, for PhAs [34], longer alkyl chain homologues had lower surface tension, which was reciprocal to the behavior of γ in homologues series of AAs [50,51] (**Figure 5(b)**). In this work, the surface tension of CAs at 298.2 K changes irregularly with the lengthening of the alkyl chain (**Figure 5(a)**). Moreover, the γ values of CAs are between the surface tension of AAs and PhAs (**Figure 5(b)**). The more detailed interpretation of S^a and S_v is given in refs. [52,78,79]. However, it should be noticed that both entropies are interpreted in terms of the surface order [79]. It can also be added that S_v, similarly like molar surface energy, concerns the sphere of volume, which consists of 1 mole of molecules. The most common value of S_v, for many organic substances is around 20 J K^{-1} mol^{-1}, due to the primarily quantum effects derived from London dispersion forces, which is the most dominant in surface tension [79]. This is also characteristic of alkanes having large molar surface entropy due to their weak mutual attraction [79]. However, as it was reported earlier [34,52], for AAs and PhAs, especially for shorter homologues S_v can achieve lower values (see **Figure 5(d)**). The molar surface entropy below 20 J K^{-1} mol^{-1} was also observed for water (8.8 J K^{-1} mol^{-1} [79]), which can be attributed to a similar order of molecules on the surface and in bulk. This is presumably possible due to the monolayer present on the surface created by hydrogen-bonded hydroxyl groups, which are bound to the surface. From **Figure 5(d)**, it is seen that the molar surface entropy of CAs resembles rather S_v of alkanes than AAs. It is maybe not very surprising when S_v of cyclohexane is 23 J K^{-1} mol^{-1} (calculated based on data from Vargaftik[80]), whereas for toluene 18 J K^{-1} mol^{-1} (calculated based on data from Badachhape [81]) and for benzene: 21.81 J K^{-1} mol^{-1} [79]. Relatively high $S_v$values of CAs show that the influence of cyclohexane on the surface properties of these substances is very strong. At the same time, the surface entropy (**Figure 5(c)**) of CAs, calculated directly from the temperature dependence of surface tension, shows the similarity to S^a of AAs with the exception of CM. It can be added that the surface entropy, S^a, of CAs increases with the lengthening of the alkyl chain, like for PhAs, whereas the S^a behaviour for AAs is quite the opposite (see **Figure 5(c)**). From the inspection of **Figures 5(b)** and **5(c)** (surface tension and surface entropy), it is obvious that the surface of CAs is ordered like for AAs, to a larger extent than it was for PhAs. This is despite the presence of cyclohexane in the molecule - a kind of steric hindrance for the creation of hydrogen bonds. To sum up, taking into account S^a - CAs seem to be closer

to AAs, whereas the normalized parameter, S_v shows the real influence of the cyclohexane of the surface layer order of CAs, which seem to be similar to alkanes (**Figure S5(c)** and **(d)**).

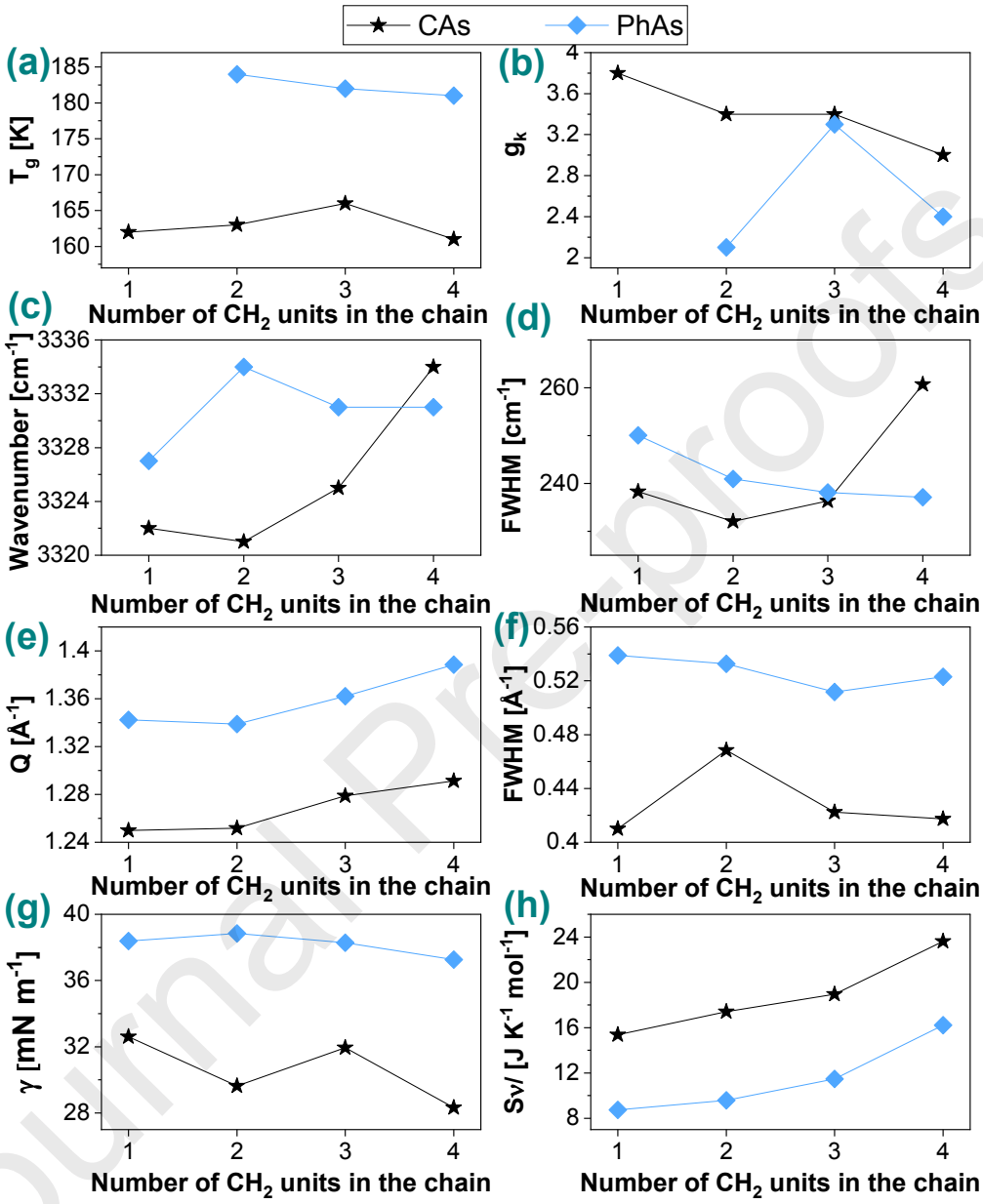

Figure 6. The effect of aromaticity and the alkyl chain length on (a) thermal, (b) dielectric (at T_g + 10 K) (c, d) infrared, (e, f) diffraction, and (g, h) surface data for the studied CAs and PhAs at T = 298 K (the error bars are within the experimental points).

In order to fully recognize the effect of the aromatic substituent in examined MAs on the H-bonding properties, the plots of different studied parameters versus the side alkyl chain length of associating liquids were constructed and presented in **Figure 6.** An interesting correlation between the Kirkwood factor and the side alkyl chain length is observed.

Generally, PhAs exhibit the non-monotonic behavior of g_K as the number of CH_2 units in the chain varies, whereas this factor decreases as the length of the side alkyl chain increases in CAs. Moreover, the T_g values for CAs are lower than those for PhAs, resembling aliphatic alcohols. FTIR results show that the replacement of a flexible cyclic ring with a rigid aromatic one modifies the spectral parameters of the ν_{OH} band. It is manifested by the changes in the intensity, the full width at half maximum, the wavenumber of the OH stretching vibration band, and the activation enthalpy for the dissociation process. FTIR data also showed that the aromatic moiety leads to larger spatial heterogeneity in H-bond strength for shorter PhAs (BA, 2C1E) compared to CAs, whereas for longer ones, there is a change in this trend. The E_a values suggested that the OH energy is sensitive to the H-bonding environment, i.e., PhAs exhibit much lower E_a values than CAs. However, in the case of PhAs, the E_a value increases with elongation of side alkyl chain length, while the non-monotonic dependence of this parameter is observed for CAs. What is more, the FWHM values of the ν_{OH}^{HB} band of PhAs at 293 K decreases with the elongation of the alkyl chain, which may indicate a gradual disappearance of the $\mathrm{O-H}\cdots\pi$ interactions (suggested by DFT calculations). It also indicates that the steric hindrance of the bulky phenyl groups in the proximity of the OH group of PhAs occur, in which aromatic rings act as intermolecular "spacers/inhibitors" for H-bonding formation. X-ray scattering data reveal damping of the pre-peak as well as broadening of the main peak and decrease in its intensity for PhAs in comparison to CAs. These features suggest that the intermolecular structure of PhAs is more complex than CAs. This is evidenced by the asymmetric shape of the main diffraction peak as well as the shift of its position towards greater Q values (shorter correlation distances) for PhAs compared to CAs. It is also seen that with the elongation of the alkyl chain, the values of the correlation distances increase. Thus, we can conclude that for longer-chained alcohols, there is a weakening of the association process. In addition, the surface tension of the studied alcohols decreases with increasing alkyl chain length, with the effect of odd-even in CAs. The values of surface entropy and molar surface entropy of CAs are higher than those of corresponding PhAs, which may be due to the slightly stronger hydrogen bonding in CAs. It should be noticed that, at first glance, the surface properties of the studied MAs (the γ, S^a, and S_v) are in apparent contradiction with the structural, thermal, and spectroscopic results. A possible reason for this is the lack of compensation of specific actions on the surface, as some molecules only come into contact with the surface. Thus, the surface effects do not have to correlate with the processes occurring in bulk.

Conclusions

In this paper, we probe the influence of aromaticity on the associating behavior of a series of non-aromatic monohydroxy alcohols and their aromatic counterparts by means of various experimental techniques, infrared and dielectric spectroscopy, X-ray diffraction, differential scanning calorimetry. Additionally, the surface tension measurements were performed, and calculations on surface entropy and molar surface entropy were made. It was found that both groups of alcohol differ in the glass transition temperature, Kirkwood factor, and the distribution of relaxation times, which indirectly imply differences in the population of hydrogen-bonding structures formed by those materials. This assumption is confirmed by IR measurements, which reveal the changes in the intensity, the full width at half maximum and wavenumber of the OH stretching vibration bandwidth, and furthermore the activation enthalpy for the dissociation. Moreover, one can add that examined CAs form the supramolecular assemblies (n) containing 3 or 4 H-bonded molecules, whereas the $n \sim 3$ for PhAs. This simply indicates that the elimination of aromaticity in the examined monohydroxy alcohols, made by a simple substitution of phenyl ring by non-aromatic cyclohexyl one, leads to some pronounced difference in the strength and the population of formed hydrogen bonds network. Also, performed XRD analysis indicated a difference in the molecular packing between both classes of materials, CAs and PhAs, as the nano-clusters created in PhAs are characterized by higher disorder between molecules. Interestingly, all results revealed that the introduction of aromaticity in the structure of monohydroxy alcohols influences the ability of these alcohols to build a hydrogen bond network and spatial organization. We believe that the presented data allow a better understanding of the behavior of self-assembling materials and the correlation between HB and chemical structure.

AUTHOR INFORMATION

NOTES. The authors declare no competing financial interests.

SUPPORTING MATERIAL. The Supporting Material file is available free of charge at http://pubs.acs.org. It contains additional figures and tables, including the results of refractive index, density, the FTIR spectra of CAs and their solutions in CCl_4 as well as the comparison of XRD data for CAs and PhAs at 293 K and T_g.

ACKNOWLEDGMENT. M.T., and N.S. are thankful for financial support from the Polish National Science Centre within the OPUS project (Dec. no 2019/33/B/ST3/00500). B.H, J.G, K.J., K.K., and S.P. are thankful for the Polish National Science Centre's financial support

within the OPUS project (Dec. no UMO-2019/35/B/ST3/02670). This research was supported in part by PLGrid Infrastructure.

REFERENCES

CRediT author statement

N. Soszka: Writing – original draft, Investigation, Formal analysis, Visualization.

B. Hachuła: Writing – original draft, Formal analysis, Methodology, Conceptualization.

M. Tarnacka: Investigation, Formal Analysis, Funding acquisition.

J. Grelska: Investigation.

K. Jurkiewicz: Investigation, Formal Analysis.

M. Geppert-Rybczyńska: Investigation, Formal Analysis.

R. Wrzalik: Investigation.

K. Grzybowska: Investigation.

S. Pawlus: Investigation, Funding acquisition.

M. Paluch: Supervision.

K. Kamiński: Methodology, Supervision.

Declaration of interests

☐ The authors declare that they have no known competing financial interests or personal relationships that could have appeared to influence the work reported in this paper.

☒ The authors declare the following financial interests/personal relationships which may be considered as potential competing interests:

Magdalena Tarnacka reports financial support was provided by National Science Centre Poland. Natalia Soszka reports financial support was provided by National Science Centre Poland. Barbara Hachula reports financial support was provided by National Science Centre Poland. Joanna Grelska reports financial support was provided by National Science Centre Poland. Karolina Jurkiewicz reports financial support was provided by National Science Centre Poland. Kamil Kaminski reports financial support was provided by National Science Centre Poland. Sebastian Pawlus reports financial support was provided by National Science Centre Poland.

- A comprehensive study on self-aggregation of monohydroxy alcohols (MAs).
- Impact of phenyl and cyclohexyl ring on the aggregation of MAs.
- Aromaticity affects the self-assembling of MAs.
- Phenyl ring introduces more heterogeneity in the organization of molecules than the cyclic one.

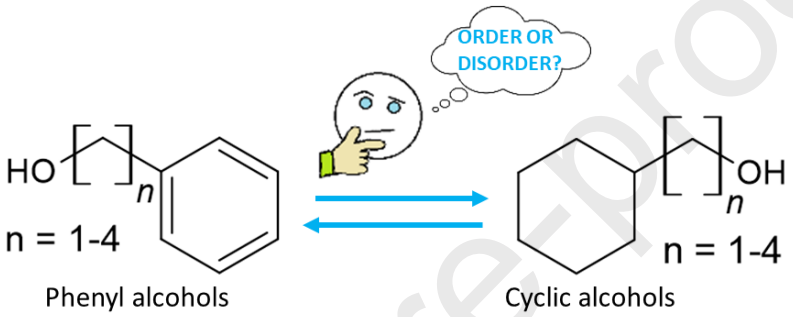

[1] E. A. Meyer, R. K. Castellano, F. Diederich, Interactions with aromatic rings in chemical and biological recognition, *Angew. Chem. Int. Ed.* 42 (2003) 1210-1250. https://doi.org/10.1002/chin.200322285

[2] W.R. Zhuang, Y. Wang, P.F. Cui, L. Xing, J. Lee, D. Kim, H.L. Jiang, Y.K. Oh, Applications of π-π stacking interactions in the design of drug-delivery systems, J. Control. Release. 294 (2019) 311–326. https://doi.org/10.1016/j.jconrel.2018.12.014.

[3] T. Chen, M. Li, J. Liu, π-π Stacking Interaction: A Nondestructive and Facile Means in Material Engineering for Bioapplications, Cryst. Growth Des. 18 (2018) 2765–2783. https://doi.org/10.1021/acs.cgd.7b01503.

[4] Z.F. Yao, J.Y. Wang, J. Pei, Control of π-π Stacking via Crystal Engineering in Organic Conjugated Small Molecule Crystals, Cryst. Growth Des. 18 (2018) 7–15. https://doi.org/10.1021/acs.cgd.7b01385.

[5] A. Banerjee, A. Saha, B.K. Saha, Understanding the Behavior of π-π Interactions in Crystal Structures in Light of Geometry Corrected Statistical Analysis: Similarities and Differences with the Theoretical Models, Cryst. Growth Des. 19 (2019) 2245–2252. https://doi.org/10.1021/acs.cgd.8b01857.

[6] D. Sharada, V.G. Saraswatula, B.K. Saha, Steering the Host Network from Cage to Channel by π···π Interactions among the Guest Molecules, Cryst. Growth Des. 18 (2018) 3719–3723. https://doi.org/10.1021/acs.cgd.8b00487.

[7] P. Bora, B. Saikia, B. Sarma, Regulation of π···π Stacking Interactions in Small Molecule Cocrystals and/or Salts for Physiochemical Property Modulation, Cryst. Growth Des. 18 (2018) 1448–1458. https://doi.org/10.1021/acs.cgd.7b01377.

[8] J.H. Deng, J. Luo, Y.L. Mao, S. Lai, Y.N. Gong, D.C. Zhong, T.B. Lu, π -π stacking interactions: Non-negligible forces for stabilizing porous supramolecular frameworks, Sci. Adv. 6 (2020) 1–9. https://doi.org/10.1126/sciadv.aax9976.

[9] C.R. Martinez, B.L. Iverson, Rethinking the term "pi-stacking," Chem. Sci. 3 (2012) 2191–2201. https://doi.org/10.1039/c2sc20045g.

[12] H.W. Roesky, M. Andruh, The interplay of coordinative, hydrogen bonding and π-π stacking interactions in sustaining supramolecular solid-state architectures. A study case of bis(4-pyridyl)- and bis(4-pyridyl-N-oxide) tectons, Coord. Chem. Rev. 236 (2003) 91–119. https://doi.org/10.1016/S0010-8545(02)00218-7.
[13] D. Vojta, M. Vazdar, The study of hydrogen bonding and π⋯π interactions in phenol⋯ethynylbenzene complex by IR spectroscopy, Spectrochim. Acta A 132 (2014) 6–14. https://doi.org/10.1016/j.saa.2014.04.149.
[14] R. Brause, M. Santa, M. Schmitt, K. Kleinermanns, Determination of the geometry change of the phenol dimer upon electronic excitation, ChemPhysChem. 8 (2007) 1394–1401. https://doi.org/10.1002/cphc.200700127.
[15] S. Yan, L.H. Spangler, Intermolecular modes of S1 p-cresol dimer; information concerning structure and dynamics, J. Phys. Chem. 95 (1991) 3915–3918. https://doi.org/10.1021/j100163a007
[16] G. Pietraperzia, M. Pasquini, F. Mazzoni, G. Piani, M. Becucci, M. Biczysko, D. Michalski, J. Bloino, V. Barone, Noncovalent interactions in the gas phase: The anisole-phenol complex, J. Phys. Chem. A. 115 (2011) 9603–9611. https://doi.org/10.1021/jp200444a.
[17] M.C. Capello, M. Broquier, C. Dedonder-Lardeux, C. Jouvet, G.A. Pino, Fast excited state dynamics in the isolated 7-azaindole-phenol H-bonded complex, J. Chem. Phys. 138 (2013) 054304. https://doi.org/10.1063/1.4789426.
[18] M.C. Capello, F.J. Hernández, M. Broquier, C. Dedonder-Lardeux, C. Jouvet, G.A. Pino, Hydrogen bonds vs. π-stacking interactions in the ρ-aminophenol. . . ρ-cresol dimer: An experimental and theoretical study, Phys. Chem. Chem. Phys. 18 (2016) 31260–31267. https://doi.org/10.1039/c6cp06352g.
[19] K. Müller-Dethlefs, P. Hobza, Noncovalent Interactions: A Challenge for Experiment and Theory, Chem. Rev. 100 (2000) 143–167. https://doi.org/10.1021/cr990033l.
[20] L. Ali, S. Sharma, B. Bezbaruah, Quantum mechanical study on the π-π stacking interaction and change in conformation of phenolic systems with different intermolecular rotations, Computational Chemistry 6 (2018) 71–86. https://doi.org/10.4236/cc.2018.64006.
[10] T.F. Headen, C.A. Howard, N.T. Skipper, M.A. Wilkinson, D.T. Bowron, A.K. Soper, Structure of π-π interactions in aromatic liquids, J. Am. Chem. Soc. 132 (2010) 5735–5742. https://doi.org/10.1021/ja909084e.
[11] A.R. Nekoei, M. Vatanparast, π-Hydrogen bonding and aromaticity: A systematic interplay study, Phys. Chem. Chem. Phys. https://doi.org/10.1039/c8cp07003b.
[21] A. Olasz, P. Mignon, F. De Proft, T. Veszprémi, P. Geerlings, Effect of the π-π Stacking interaction on the acidity of phenol, Chem. Phys. Lett. 407 (2005) 504–509. https://doi.org/10.1016/j.cplett.2005.03.145.
[22] S. Pérez-Casas, R. Moreno-Esparza, M. Costas, D. Patterson, Effect of steric hindrance and π electrons on alcohol self-association, J. Chem. Soc. Faraday Trans. 87 (1991) 1745–1750. https://doi.org/10.1039/FT9918701745.
[23] G.P. Johari, O.E. Kalinovskaya, J.K. Vij, Effects of induced steric hindrance on the dielectric behavior and H bonding in the supercooled liquid and vitreous alcohol, J. Chem. Phys. 114 (2001) 4634–4642. https://doi.org/10.1063/1.1346635.
[24] K. Shin-ya, H. Sugeta, S. Shin, Y. Hamada, Y. Katsumoto, K. Ohno, Absolute configuration and conformation analysis of 1-phenylethanol by matrix-isolation infrared and vibrational circular dichroism spectroscopy combined with density functional theory calculation, J. Phys. Chem. A. 111 (2007) 8598–8605. https://doi.org/10.1021/jp068448v.
[25] M. Mons, E.G. Robertson, J.P. Simons, Intra- and Intermolecular π-Type Hydrogen Bonding in Aryl Alcohols: UV and IR-UV Ion Dip Spectroscopy, J. Phys. Chem. A. 104 (2000) 1430–1437. https://doi.org/10.1021/jp993178k.
[26] T T. Böhmer, J.P. Gabriel, T. Richter, F. Pabst, T. Blochowicz, Influence of Molecular Architecture on the Dynamics of H-Bonded Supramolecular Structures in Phenyl-Propanols, J. Phys. Chem. B. 123 (2019) 10959–10966. https://doi.org/10.1021/acs.jpcb.9b07768.
[27] K. Jurkiewicz, S. Kołodziej, B. Hachuła, K. Grzybowska, M. Musiał, J. Grelska, R. Bielas, A. Talik, S. Pawlus, K. Kamiński, M. Paluch, Interplay between structural static and dynamical parameters as a key factor to understand peculiar behaviour of associated liquids, J. Mol. Liq. 319 (2020) 114084. https://doi.org/10.1016/j.molliq.2020.114084.
[28] S. Kołodziej, J. Knapik-Kowalczuk, K. Grzybowska, A. Nowok, S. Pawlus, Essential meaning of high pressure measurements in discerning the properties of monohydroxy alcohols with a single phenyl group, J. Mol. Liq. 305 (2020) 112863. https://doi.org/10.1016/j.molliq.2020.112863.
[29] A. Nowok, K. Jurkiewicz, M. Dulski, H. Hellwig, J.G. Małecki, K. Grzybowska, J. Grelska, S. Pawlus, Influence of molecular geometry on the formation, architecture and dynamics of H-bonded supramolecular associates in 1-phenyl alcohols, J. Mol. Liq. 326 (2021) 115349. https://doi.org/10.1016/j.molliq.2021.115349.
[30] A. Nowok, M. Dulski, K. Jurkiewicz, J. Grelska, A.Z. Szeremeta, K. Grzybowska, S. Pawlus, Molecular stiffness and aromatic ring position – crucial structural factors in the self-assembly processes of phenyl alcohols, J. Mol. Liq. (2021) 116426. https://doi.org/10.1016/j.molliq.2021.116426.

[31] A. Nowok, M. Dulski, J. Grelska, A.Z. Szeremeta, K. Jurkiewicz, K. Grzybowska, M. Musiał, S. Pawlus, Phenyl Ring: A Steric Hindrance or a Source of Different Hydrogen Bonding Patterns in Self-Organizing Systems?, J. Phys. Chem. Lett. 12 (2021) 2142–2147. https://doi.org/10.1021/acs.jpclett.1c00186.
[32] J.P. Gabriel, E. Thoms, R. Richert, High electric fields elucidate the hydrogen-bonded structures in 1-phenyl-1-propanol, J. Mol. Liq. 330 (2021) 115626. https://doi.org/10.1016/j.molliq.2021.115626.
[33] B. Hachuła, J. Grelska, N. Soszka, K. Jurkiewicz, A. Nowok, A.Z. Szeremeta, S. Pawlus, M. Paluch, K. Kaminski, Systematic studies on the dynamics, intermolecular interactions and local structure in the alkyl and phenyl substituted butanol isomers, J. Mol. Liq. (2021) 117098. https://doi.org/10.1016/j.molliq.2021.117098.
[34] N. Soszka, B. Hachuła, M. Tarnacka, E. Ozimina-Kamiska, J. Grelska, K. Jurkiewicz, M. Geppert-Rybczynska, R. Wrzalik, K. A. Grzybowska, S. Pawlus, M. Paluch, K. Kaminski, The impact of the length of alkyl chain on the behavior of benzyl alcohol homologous. The interplay between dispersive and hydrogen bond interaction. Phys. Chem. Chem. Phys. 23 (2021) 23796-23807. https://doi.org/10.1039/D1CP02802B.
[35] S. Mustafa, L.A. Dissado, R.M. Hill, Structure and Dipole Relaxation Mechanisms in the Cyclic Alcohols Cyclopentanol to Cyclo-octanol, J. Chem. Soc. Faraday Trans. 79 (1983) 369–417. https://doi.org/10.1039/F29837900369
[36] M. Tyagi, S.S.N. Murthy, Study of the nature of glass transitions in the plastic crystalline phases of cyclo-octanol, cycloheptanol, cyanoadamantane and cis-1,2-dimethylcyclohexane, J. Chem. Phys. 114 (2001) 3640–3652. https://doi.org/10.1063/1.1342811.
[37] M.P. Nighil Nath, M.K. Sulaiman, M.S. Thayyil, Thermal & dielectric spectroscopic investigation on orientationaly disordered crystal-cyclobutanol, Mater. Today Proc. 18 (2019) 1620–1626. https://doi.org/10.1016/j.matpr.2019.05.256.
[38] R. Brand, P. Lunkenheimer, A. Loidl, Relaxations and fast dynamics of the plastic crystal cyclo-octanol investigated by broadband dielectric spectroscopy, Phys. Rev. B - Condens. Matter Mater. Phys. 56 (1997) R5713–R5716. https://doi.org/10.1103/PhysRevB.56.R5713.
[39] R. Brand, P. Lunkenheimer, A. Loidl, Relaxation dynamics in plastic crystals, J. Chem. Phys. 116 (2002) 10386–10401. https://doi.org/10.1063/1.1477186.
[40] S. Havriliak, S. Negami, A complex plane analysis of α-dispersions in some polymer systems, J. Polym. Sci. Part C Polym. Symp. 14 (1966) 99–117. https://doi.org/10.1002/polc.5070140111.
[41] F. Kremer, A. Schonhals, Broadband Dielectric Spectroscopy, Springer, Berlin, 2003.
[42] F. Alvarez, A. Alegra, J. Colmenero, Relationship between the time-domain Kohlrausch-Williams-Watts and frequency-domain Havriliak-Negami relaxation functions, Phys. Rev. B. 44 (1991) 7306–7312. https://doi.org/10.1103/PhysRevB.44.7306.
[43] G. Williams, D.C. Watts, Non-symmetrical dielectric relaxation behaviour arising from a simple empirical decay function, Trans. Faraday Soc. 66 (1970) 80–85. https://doi.org/10.1039/TF9706600080.
[44] R. Kohlrausch, Ueber das Dellmann'sche Elektrometer, Ann. Phys. 72 (1847) 353−405. https://doi.org/10.1002/andp.18471481102
[45] H. Vogel, Das temperaturabhängigkeitsgesetz der viskosität von flüssigkeiten, J. Phys. Z. 22 (1921) 645–646.
[46] G.S. Fulcher, Analysis of Recent Measurements of the Viscosity of Glasses, J. Am. Ceram. Soc. 8 (1925) 339–355. https://doi.org/10.1111/j.1151-2916.1925.tb16731.x..
[47] G. Tammann, W. Hesse, Die abhängigkeit der viscosität von der temperatur bie unterkühlten flüssigkeiten, Z. Anorg. Allg. Chem. 156 (1926) 245–257. https://doi.org/10.1002/zaac.19261560121.
[48] A. Wandschneider, J.K. Lehmann, A. Heintz, Surface Tension and Density of Pure Ionic Liquids and Some Binary Mixtures with 1-Propanol and 1-Butanol, J. Chem. Eng. Data. 53 (2008) 596–599. https://doi.org/10.1021/je700621d
[49] J. Feder-Kubis, M. Geppert-Rybczyńska, M. Musiał, E. Talik, A. Guzik, Exploring the surface activity of a homologues series of functionalized ionic liquids with a natural chiral substituent: (-)-menthol in a cation, Colloids Surf. A Physicochem. Eng. Asp. 529 (2017) 725–732. https://doi.org/10.1016/j.colsurfa.2017.06.040
[50] G. Vázquez, E. Alvarez, J.M. Navaza, Surface tension of alcohol + water from 20 to 50 °C, J. Chem. Eng. Data 40 (1995) 611—614. https://doi.org/10.1021/je00019a016
[51] Yu.V. Efremov, Density, surface tension, saturation vapor pressure, and critical parameters of alcohols, Zh. Fiz. Khim. 40 (1996) 1240–1247.
[52] R.T. Myers, True molar surface energy and alignment of surface molecules, J. Colloid Interface Sci. 274 (2004) 229–236. https://doi.org/10.1016/j.jcis.2003.12.048.
[53] Gaussian 09, Revision A.02, M. J. Frisch, G. W. Trucks, H. B. Schlegel, G. E. Scuseria, M. A. Robb, J. R. Cheeseman, G. Scalmani, V. Barone, G. A. Petersson, H. Nakatsuji, X. Li, M. Caricato, A. Marenich, J. Bloino, B. G. Janesko, R. Gomperts, B. Mennucci, H. P. Hratchian, J. V. Ortiz, A. F. Izmaylov, J. L. Sonnenberg, D. Williams-Young, F. Ding, F. Lipparini, F. Egidi, J. Goings, B. Peng, A. Petrone, T. Henderson, D. Ranasinghe, V. G. Zakrzewski, J. Gao, N. Rega, G. Zheng, W. Liang, M. Hada, M. Ehara, K. Toyota, R. Fukuda, J.

Hasegawa, M. Ishida, T. Nakajima, Y. Honda, O. Kitao, H. Nakai, T. Vreven, K. Throssell, J. A. Montgomery, Jr., J. E. Peralta, F. Ogliaro, M. Bearpark, J. J. Heyd, E. Brothers, K. N. Kudin, V. N. Staroverov, T. Keith, R. Kobayashi, J. Normand, K. Raghavachari, A. Rendell, J. C. Burant, S. S. Iyengar, J. Tomasi, M. Cossi, J. M. Millam, M. Klene, C. Adamo, R. Cammi, J. W. Ochterski, R. L. Martin, K. Morokuma, O. Farkas, J. B. Foresman, and D. J. Fox, Gaussian, Inc., Wallingford CT, 2016.

[54] S. F. Boys, F. Bernardi, Mol. Phys. 19 (1970) 553–566. https://doi.org/10.1080/00268977000101561.

[55] V.N. Novikov, E.A. Rössler, Correlation between glass transition temperature and molecular mass in non-polymeric and polymer glass formers, Polymer. 54 (2013) 6987–6991. https://doi.org/10.1016/j.polymer.2013.11.002.

[56] R. Böhmer, C. Gainaru, R. Richert, Structure and dynamics of monohydroxy alcohols-Milestones towards their microscopic understanding, 100 years after Debye, Phys. Rep. 545 (2014) 125–195. https://doi.org/10.1016/j.physrep.2014.07.005.

[57] M. Wikarek, S. Pawlus, S.N. Tripathy, A. Szulc, M. Paluch, How different molecular architectures influence the dynamics of H-bonded structures in glass-forming monohydroxy alcohols. J. Phys. Chem. B 120 (2016) 5744−5752. https://doi.org/10.1021/acs.jpcb.6b01458.

[58] T. Büning, J. Lueg, J. Bolle, C. Sternemann, C. Gainaru, M. Tolan, R. Böhmer, Connecting structurally and dynamically detected signatures of supramolecular Debye liquids, J. Chem. Phys. 147 (2017) 234501. https://doi.org/10.1063/1.4986866.

[59] L.M. Wang, R. Richert, Dynamics of glass-forming liquids. IX. Structural versus dielectric relaxation in monohydroxy alcohols, J. Chem. Phys. 121 (2004) 11170–11176. https://doi.org/10.1063/1.1811072.

[60] C. Brot, M. Magat, Comment on “dispersion at millimeter wavelengths in methyl and ethyl alcohols”, J. Chem. Phys. 39 (1963) 841–842. https://doi.org/10.1063/1.1734336.

[61] O.E. Kalinovskaya, J.K. Vij, The exponential dielectric relaxation dynamics in a secondary alcohol’s supercooled liquid and glassy states, J. Chem. Phys. 112 (2000) 3262–3266. https://doi.org/10.1063/1.480909.

[62] V. V Levin, Y.D. Feldman, Dipole relaxation in normal aliphatic alcohols, Chem. Phys. Lett. 87 (1983) 162–164. https://doi.org/10.1016/0009-2614(82)83579-3.

[63] P.M. Déjardin, S. V. Titov, Y. Cornaton, Linear complex susceptibility of long-range interacting dipoles with thermal agitation and weak external ac fields, Phys. Rev. B. 99 (2019) 1–14. https://doi.org/10.1103/PhysRevB.99.024304.

[64] N. Soszka, B. Hachuła, M. Tarnacka, E. Kaminska, S. Pawlus, K. Kaminski, M. Paluch, Is a Dissociation Process Underlying the Molecular Origin of the Debye Process in Monohydroxy Alcohols?, J. Phys. Chem. B. 125 (2021) 2960–2967. https://doi.org/10.1021/acs.jpcb.0c10970.

[65] L.P. Singh, R. Richert, Watching hydrogen-bonded structures in an alcohol convert from rings to chains, Phys. Rev. Lett. 109 (2012) 1–5. https://doi.org/10.1103/PhysRevLett.109.167802.

[66] J.G. Kirkwood, The dielectric polarization of polar liquids, J. Chem. Phys. 7 (1939) 911–919. https://doi.org/10.1063/1.1750343.

[67] W. Dannhauser, R. H. Cole, Dielectric properties of liquid butyl alcohols, *J. Chem. Phys*. 23 (1955) 1762–1766. https://doi.org/10.1063/1.1740576

[68] W. Dannhauser, Dielectric study of intermolecular association in isomeric octyl alcohols, J. Chem. Phys. 48 (1968) 1911–1917. https://doi.org/10.1063/1.1668989.

[69] W. Dannhauser, R.H. Cole, Dielectric properties of liquid butyl alcohols, J. Chem. Phys. 23 (1955) 1762–1766. https://doi.org/10.1063/1.1740576.

[70] C.P. Johari, W. Dannhauser, Dielectric study of the pressure dependence of intermolecular association in isomeric octyl alcohols, J. Chem. Phys. 48 (1968) 5114–5122. https://doi.org/10.1063/1.1668182.

[71] B.N. Solomonov, V.B. Novikov, M.A. Varfolomeev, A.E. Klimovitskii, Calorimetric determination of hydrogen-bonding enthalpy for neat aliphatic alcohols, J. Phys. Org. Chem. 18 (2005) 1132–1137. https://doi.org/10.1002/poc.977.

[72] M. Kwaśniewicz, M.A. Czarnecki, The Effect of Chain Length on Mid-Infrared and Near-Infrared Spectra of Aliphatic 1-Alcohols, Appl. Spectrosc. 72 (2018) 288–296. https://doi.org/10.1177/0003702817732253.

[73] R. Hayes, S. Imberti, G. G. Warr, R. Atkin, Effect of cation alkyl chain length and anion type on protic ionic liquid nanostructure, J. Phys. Chem. C 118 (2014) 13998−14008. https://doi.org/10.1021/jp503429k.

[74] A.K. Karmakar, P.S.R. Krishna, R.N. Joarder, On the structure function of liquid alcohols at small wave numbers and signature of hydrogen-bonded clusters in the liquid state, Phys. Lett. Sect. A Gen. At. Solid State Phys. 253 (1999) 207–210. https://doi.org/10.1016/S0375-9601(99)00038-9.

[75] A. Perera, F. Sokolić, L. Zoranić, Microstructure of neat alcohols, Phys. Rev. E - Stat. Nonlinear, Soft Matter Phys. 75 (2007) 1–4. https://doi.org/10.1103/PhysRevE.75.060502.

[76] L. Almásy, A.I. Kuklin, M. Požar, A. Baptista, A. Perera, Microscopic origin of the scattering pre-peak in aqueous propylamine mixtures: X-ray and neutron experiments: Versus simulations, Phys. Chem. Chem. Phys. 21 (2019) 9317–9325. https://doi.org/10.1039/c9cp01137d.
[77] A. Ghoufi, Molecular origin of the prepeak in the structure factor of alcohols, J. Phys. Chem. B. 124 (2020) 11501–11509. https://doi.org/10.1021/acs.jpcb.0c09302.
[78] J. Lyklema, A discussion on surface excess entropies, Colloids Surfaces A Physicochem. Eng. Asp. 186 (2001) 11–16. https://doi.org/10.1016/S0927-7757(01)00477-0.
[79] L. Glasser, Volume-based thermodynamics of organic liquids: Surface tension and the Eötvös equation, J. Chem. Thermodyn. 157 (2021) 106391. https://doi.org/10.1016/j.jct.2021.106391.
[80] N. B. Vargaftik, Thermophysical Properties of Gases and Liquids, A Reference Book. Nauka, Moscow, 1972.
[81] R. B. Badachhape, M. K. Gharpurey, A. B. Biswas, Density and surface tension of phenol, (mono-, di-, and tri-)-chlorophenols, salol, and (o- and m-) chloronitrobenzenes, J. Chem. Eng. Data 10 (1965) 43-145. https://doi.org/10.1021/je60025a022.